Spectrochimica Acta Part A: Molecular and Biomolecular Spectroscopy 303 (2023) 123153

Contents lists available at ScienceDirect

Spectrochimica Acta Part A: Molecular and Biomolecular Spectroscopy

journal homepage: www.journals.elsevier.com/spectrochimica-acta-part-a-molecular-and-biomolecular-spectroscopy

Ag microlabyrinth/nanoparticles coated large-area thin PDMS films as flexible and transparent SERS substrates for in situ detection

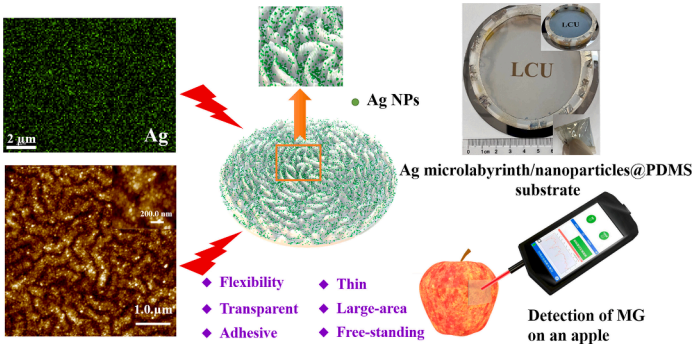
Meng Sun [a], Houjia Zhang [a], Hefu Li [a,*], Xuehui Hao [b], Changzheng Wang [b], Lijun Li [a], Zhenshan Yang [a], Cunwei Tian [a,*]

[a] School of Physical Science and Information Technology, Key Laboratory of Optical Communication Science and Technology of Shandong Province, Liaocheng University, Liaocheng, 252000, China
[b] School of Materials Science and Engineering, Liaocheng University, Liaocheng, 252000, China

HIGHLIGHTS

- Large-scale and cost-effective fabrication method to prepare flexible and transparent SERS substrates was proposed.
- The thin, free-standing SERS substrate consists of ALNHS decorated PDMS film.
- The ALNHS induced plentiful multiple-type hot spots.
- The excellent SERS performance of the ALNHS@PDMS film was demonstrated.
- In situ detection of malachite green on apple and tomato skin was readily performed with a portable Raman spectrometer.

GRAPHICAL ABSTRACT



ARTICLE INFO

Keywords:
SERS
thin PDMS films
Ag hierarchical structures
Pesticides
In situ detection

ABSTRACT

Flexible and transparent surface-enhanced Raman scattering (SERS) substrates have attracted much attention as a fast, sensitive and in situ detection platform for practical applications. However, the large-area fabrication of flexible and transparent SERS substrates with high performance is still challenging. Here, a flexible and transparent SERS substrate based on large-area thin PDMS film decorated with Ag microlabyrinth/nanoparticles hierarchical structures (denoted as ALNHS@PDMS) is fabricated by using the floating-on-water method and magnetron sputtering technology. By optimizing the sputtering time, the ALNHS with multiple hot spots are uniformly distributed on the PDMS surface. Based on characterizing the rhodamine 6G (R6G) with a portable Raman spectrometer, the optimal ALNHS@PDMS film exhibits a high enhancement factor (5.2×10^6), excellent uniformity and reproducibility, as well as superior mechanical stability. In addition, thanks to the good sticky feature and bi-directional activation property of the thin ALNHS@PDMS film, the prepared flexible and transparent SERS substrate can achieve in situ detection of malachite green residues (10^{-6} M) on apple and tomato skins. This large-area, thin, mechanically robust, flexible and transparent ALNHS@PDMS film, integrated with a portable Raman spectrometer, shows great potential for point-of-care testing (POCT) in practical applications.

* Corresponding authors.
E-mail addresses: lihefu@lcu.edu.cn, tiancw2008@163.com (C. Tian).

https://doi.org/10.1016/j.saa.2023.123153
Received 9 February 2023; Received in revised form 28 June 2023; Accepted 12 July 2023
Available online 13 July 2023
1386-1425/© 2023 Published by Elsevier B.V.

1. Introduction

Surface-enhanced Raman scattering (SERS) provides a label-free, rapid, and sensitive detection technology for trace biochemical analytes in various fields [1–8]. It is now generally accepted that the significantly amplified Raman signals of molecules mainly depend on electromagnetic enhancement, and it especially occurs at the sharp tips or nanogaps of metallic nanostructures (so called "hot spots") [9–11]. Thus, engineering uniform and dense hot spots in plasmonic nanostructures is a prerequisite for high-performance SERS substrates [12,13]. Traditional SERS substrates usually utilize brittle and/or rigid substrates as supporting materials of metallic nanostructures [14–16]. Although highly sensitive and reproducible detection can be achieved, the rigid SERS substrates are not suitable for direct detection of analytes adsorbed on curved surfaces due to the lack of flexibility, limiting their point-of-care testing (POCT) applications [17,18].

Currently, flexible SERS substrates have received great attention for POCT applications because they can quickly collect and detect analytes on nonplanar surfaces [19]. To date, soft materials such as papers [20–22], polymer films [23,24], textile fabrics [25,26], and tapes [27,28] have been used to fabricate flexible SERS substrates. The material flexibility enables conformal contact between SERS substrates and irregular object surfaces and allows for the quick, effective, and nondestructive detection [29,30]. Especially, the flexible and transparent polymer films, e.g., poly (methyl methacrylate) (PMMA) [31], poly (vinylidene fluoride) (PVDF) [32], polydimethylsiloxane (PDMS) [33], polyethylene terephthalate (PET) [34], and poly-(vinyl chloride) (PVC) [35], have been considered as better alternatives. The combination of flexibility and transparency endows the adaptability of SERS substrates for nonplanar surfaces and enables the in situ detection [36]. In this regard, these flexible and transparent SERS substrates combined with portable Raman analyzers can provide tremendous convenience in on-site, real-time monitoring of targeted analytes in real-word objects [18]. As a result, constructing flexible and transparent SERS substrates with high performance is of paramount importance for POCT applications.

PDMS is one of the most widely used polymer materials for preparing flexible and transparent SERS substrates, due to its advantages of high transparency, good tensile strength, and inert and nontoxic properties [37]. There have been some methods for preparation of PDMS-based SERS substrates, such as in situ synthesis [38,39], self-assembly [40,41] and seeding deposition [42]. However, these strategies are time-consuming and complex, and suffer from large-area fabrication, such that high-throughput production of SERS substrates cannot be achieved. Thus, it is highly desirable to develop a methodology for low-cost fabrication of flexible SERS substrates with batch-to-batch consistency and large-scale production. In this respect, magnetron sputtering is a more ideal technique for fabricating large-area SERS substrates [33,43,44], as it allows for rapid fabrication of uniform and controllable plasmonic nanostructures with excellent reproducibility [45]. Besides, for highly sensitive in situ detection, two challenges still need to be overcome. Firstly, there is a requirement for constructing plenty of hot spots on the top of the PDMS film for better accessibility to target analytes. Secondly, the thickness of the PDMS film should be thin for achieving conformal coverage on complex, irregular target surfaces. Therefore, it is essential to develop a facile, yet efficient approach to fabricate large-area, flexible and transparent SERS substrate which can generate high-density and highly accessible hot spots on the top surface of thin supporting substrates.

Here, to address the above issues, we present a facile strategy to fabricate high- performance SERS substrates with excellent flexibility and optical transparency. More importantly, the large-area, thin, free-standing SERS substrate can be prepared in a reliable and reproducible manner. The flexible and transparent SERS substrate consists of Ag microlabyrinth/nanoparticles hierarchical structures (ALNHS) on a thin PDMS film, which is denoted as ALNHS@PDMS film. Taking advantages of the extremely flat surface of water, the large-scale, thin PDMS film was fabricated by the floating-on-water method. The highly uniformly distributed ALNHS was successfully coated on the PDMS film through magnetron sputtering technology. By optimizing the sputtering time, the optimal ALNHS@PDMS film with a total thickness of ~ 100 μm demonstrates high sensitivity, superior uniformity and reproducibility, as well as excellent mechanical stability and storage stability. Because of plenty of SERS hot spots resulting from multiple plasmon couplings in the ALNHS and thin thickness of the PDMS film, the ALNHS@PDMS film realizes in situ detection with a limit of detection of 10^{-6} M for malachite green on the contaminated apple and tomato skin. It is also worth noting that the as-prepared flexible ALNHS@PDMS film with high performance, in combination with a portable Raman analyzer, can meet the on-site, real-time detection requirement in POCT applications.

2. Materials and methods

2.1. Materials

Silver target (purity: 99.999%) was purchased from Zhongnuo Advanced Material Technology Co., Ltd. Polydimethylsiloxane (PDMS) was bought from Hangzhou Jingbo Technology Co., Ltd. Rhodamine 6G (R6G) was purchased from Sigma-Aldrich. Crystal violet (CV) and malachite green (MG) were obtained from Aladdin Reagent (Shanghai) Co., Ltd. Deionized (DI) water was used to prepare aqueous solutions.

2.2. Preparation of large-area ALNHS@PDMS thin film

The fabrication process of large-area ALNHS@PDMS thin film is illustrated in Scheme 1. Firstly, the large-area PDMS thin film was prepared through a floating-on-water method [46]. The PDMS base and the curing agent at a weight ratio of 10:1 were mixed by mechanical agitation for 20 min. The mixed solution was then placed in a vacuum drying oven for 30 min to remove bubbles and poured onto the deionized water in a petri dish with a diameter of 10 cm. Since the mixture is immiscible with water and its density is smaller than that of water, the mixture floated and spread on the water surface. After curing at room temperature for one day, crosslinking reaction of base and curing agent had finished, and a large-area and flat PDMS film with a thickness of ~ 100 μm was picked up from the water surface using a polypropylene hollow ring, which can avoid plastic deformation of the PDMS film to ensure the film flatness. To remove the water from the PDMS surface, the film was cured at 55 °C for 3 h.

Secondly, the as-prepared PDMS film was decorated with ALNHS using a magnetron sputtering apparatus (TRP450, SKY Technology Development Co., Ltd, China). During the deposition process, the DC power, base, and working pressure were 20 W, 5.0×10^{-4}, and 0.8 Pa, respectively. In addition, the sample holder was rotated at a speed of 10 rpm. The deposition times were set as 40, 45 and 50 s.

2.3. Characterizations

The as-prepared SERS substrates were characterized by atomic force microscopy (AFM, Bruke Icon), scanning electron microscopy (SEM, Apero S HiVac), and UV − vis spectroscopy (Hitachi U-3310, Japan). The surface hydrophilicity of the pure PDMS film and the flexible SERS substrate was measured using a contact angle meter (Kruss DSA25S, Germany). The SERS spectra were collected at room temperature using a smartphone-based Raman analyzer (ATR6500, Optosky photoelectric Co., Ltd., China) with a laser of 785 nm (20 mW power) and acquisition time of 10 s. The SERS mappings were measured using the Renishaw inVia Raman system with a laser of 785 nm (100% power) and acquisition time of 2 s.

2.4. SERS measurements

To evaluate the SERS activity of ALNHS@PDMS substrates, R6G, MG, and CV were selected as reported molecules and dissolved in DI water for preparing aqueous solutions of different concentrations. 5 μL of their aqueous solutions were dropped on the SERS substrate and dried naturally. SERS measurements were performed using a portable Raman analyzer. For in situ detection of pesticide residues, 20 μL of MG solution with different concentrations was dropped on the apple and tomato surfaces and dried in air. Then, the ALNHS@PDMS film was placed on the pesticide-contaminated skin with ALNHS facing the target surface for direct SERS measurement using a portable Raman spectrometer (Scheme 1).

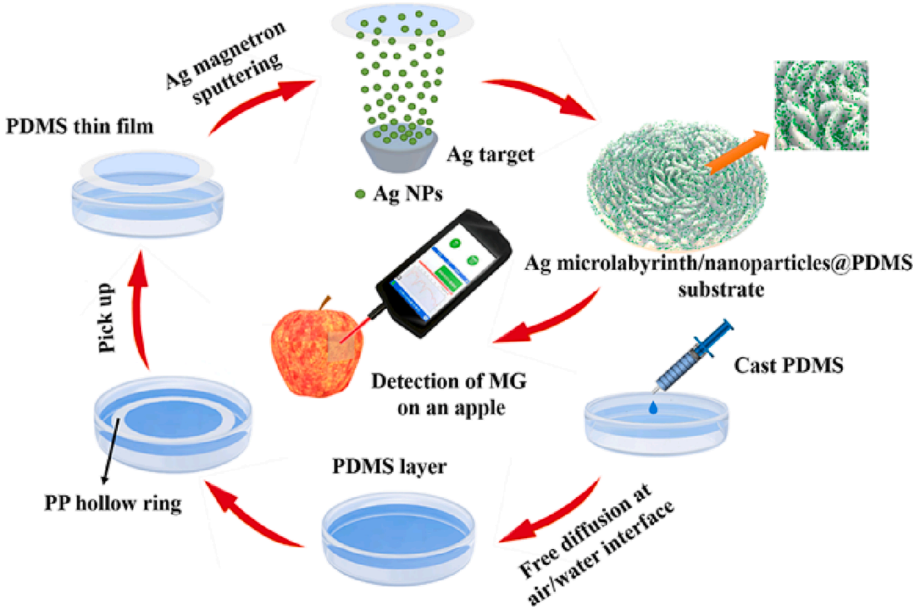
3. Results and discussion

3.1. Fabrication and characterization of large-area ALNHS@PDMS thin film

To achieve ultrasensitive in situ detection, the accessibility between plasmonic nanostructures and object surfaces is a critical factor. Thus, it is necessary to reduce the flexible film thickness to obtain good conformal contact. Although the spin-coating method can fabricate PDMS films with thickness down to several micrometers, their strong interaction with underlying substrates makes them difficult to realize large-area damage-free transfer. Thus, this method is not available for easily preparing thin PDMS film across a large area. Herein, a large-area PDMS thin film is prepared by the floating-on-water method utilizing the immiscibility between PDMS solution and water. After curing, the large-area thin PDMS film can be readily peeled off from the water, and the as-fabricated PDMS film has a large area of ~ 41 cm^2 (left panel of Fig. 1a). It can be seen that the blank PDMS film exhibits high transparency as the LCU letters on the paper under the PDMS film can be clearly seen. After Ag coating, the color of the pure PDMS film changes from white to brown or gray at different viewing angles, as shown in the right panel of Fig. 1a. The uniform color and luster indicate that the PDMS film has been successfully embellished with a homogeneous Ag layer. Additionally, it demonstrates that the Ag-coated PDMS film exhibits high-transparency. The excellent flexibility of the Ag-coated PDMS film can be confirmed by folding it into different shapes, as shown in Fig. 1b-d. Therefore, the above results reveal that the large-area Ag-coated PDMS film with excellent transparency and flexibility can be easily fabricated by combination of the floating-on-water method and magnetron sputtering technology.

To investigate the morphologies of Ag-coated PDMS films under different deposition times varying from 40 to 50 s with an interval of 5 s, the SEM images of Ag-coated PDMS films are exhibited in Fig. 2a-c. It can be clearly observed that the randomly oriented wrinkles were produced in all PDMS-supported Ag films, forming labyrinth pattern. From the corresponding AFM images in Fig. 2d-f, it can be seen that all three wrinkles are large labyrinth-like patterns with small nanoparticle structures. The wrinkle wavelength and amplitude increase with increasing deposition time, which is in accordance with previous reports [47]. In addition, elliptical Ag NPs are formed on PDMS film surface due to the Volmer–Weber (VW) growth. At a low deposition time (40 s), the Ag NPs were able to nucleate and grow. With increasing deposition time (45 s), the average size of Ag NPs increased and the gap between neighboring particles decreased, leading to high-density hot spots in the Ag film. For a larger deposition time (50 s), the coalescence between adjacent Ag NPs reduces the number of gaps. The as-fabricated flexible SERS substrate with 40, 45, and 50 s sputtering time were denoted as ALNHS-40@PDMS, ALNHS-45@PDMS, and ALNHS-50@PDMS, respectively. These SERS-active ALNHS are highly suitable for constructing hot spots with improved intensity and high density over the whole surface resulting from localized surface plasmon resonance (LSPR) through interparticle interactions.

The total thickness of ALNHS-45@PDMS film is ~ 100 μm, as depicted in Fig. 3a, which can enable conformal contact with the object surface for closer accessibility to the analytes. The UV − vis spectrum in Fig. 3b shows that a broad band from 500 to 800 nm, which might be due to the strong plasmonic coupling between neighboring Ag NPs and/or nanoparticle-film interactions. Therefore, the ALNHS-45@PDMS substrate could offer abundant hot spots and strong electromagnetic field enhancement. The energy-dispersive spectroscopy (EDS) spectra of the ALNHS-45@PDMS film is illustrated in Fig. 3c. Apart from the characteristic peaks of Si, O and C elements from the PDMS film and Pt element from a Pt thin layer sputtered onto the sample, the strong peak of the Ag element can be observed in the EDS spectra, which indicates that the Ag layer were coated on the surface of PDMS film. The distribution of Ag NPs on the surface of the PDMS film was investigated by



Scheme 1. Preparation process of the Ag microlabyrinth/nanoparticles coated large-area thin PDMS film, and the corresponding POCT analysis of pesticide residues on the agricultural product using a portable Raman analyzer.

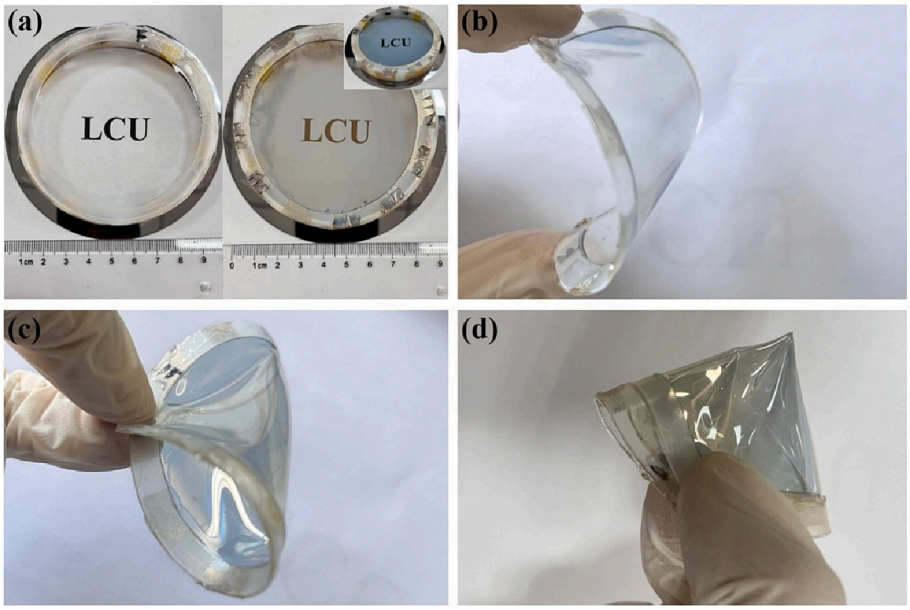


Fig. 1. (a) Photographs of the as-fabricated thin PDMS film using the floating-on-water method (left) and the PDMS film after Ag coating (right) placed on the paper printed with letters of LCU, (b-d) Photographic images of the Ag-coated PDMS film for a sputtering time of 45 s under bending and folding states.

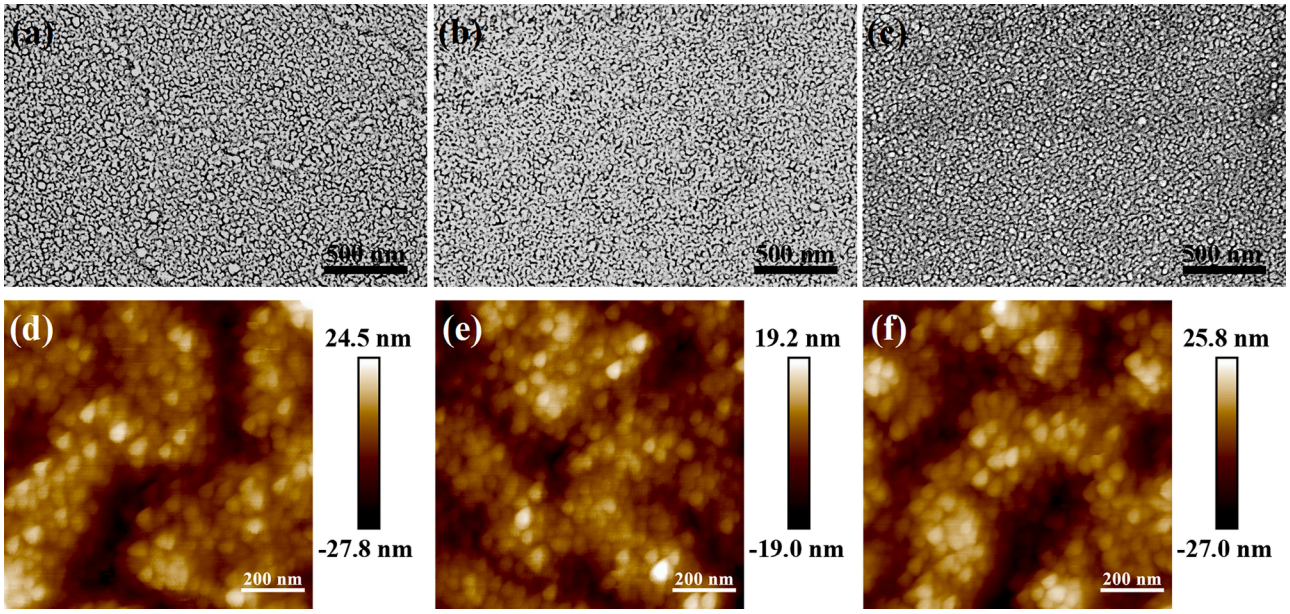


Fig. 2. SEM images of the Ag-coated PDMS film with the deposition time of (a) 40 s, (b) 45 s, (c) 50 s. (d-f) AFM images of Ag-coated PDMS film for deposition time of 40, 45, and 50 s, respectively.

EDS mapping, as shown in Fig. 3d. The figure shows that the Ag NPs are homogeneously distributed on the PDMS surface. These results clearly confirm the successful deposition of homogeneous Ag layer on the PDMS film. The wettability of the ALNHS-45@PDMS film was investigated by the water contact angle (WCA) measurement. Compared with the WCA (~107°) of the pure PDMS film (Fig. 3e), the WCA (~110°) of the ALNHS-45@PDMS film is slightly larger (Fig. 3f), which can aggregate analytes to improve the SERS sensitivity [48].

3.2. SERS performance of ALNHS@PDMS films

To evaluate the SERS performance of the ALNHS@PDMS films fabricated with different sputtering times, R6G was chosen as the probe molecule. The SERS spectra of 10^{-5} M R6G collected on the different ALNHS@PDMS films are shown in Fig. 4a. For all of the flexible SERS substrates, the characteristic bands of R6G at 612, 774, 1183, 1315, 1362, and 1510 cm^{-1} are clearly observed, which are in accordance with the previous report [49]. In addition, one can see that the difference in Raman signal intensities of R6G on different SERS substrates is very obvious. The Raman intensity at 1510 cm^{-1} versus sputtering time is shown in the inset of Fig. 4a. It clearly reveals that the strongest Raman signal is obtained on the ALNHS-45@PDMS film. This result suggests that ALNHS-45@PDMS film is the optimal flexible SERS substrate in this series of samples, and thus it is used in the subsequent SERS measurements.

The sensitivity of the ALNHS-45@PDMS film was investigated by Raman spectra analysis of R6G solution with various concentrations. Fig. 4b displays the SERS spectra of R6G with different concentrations

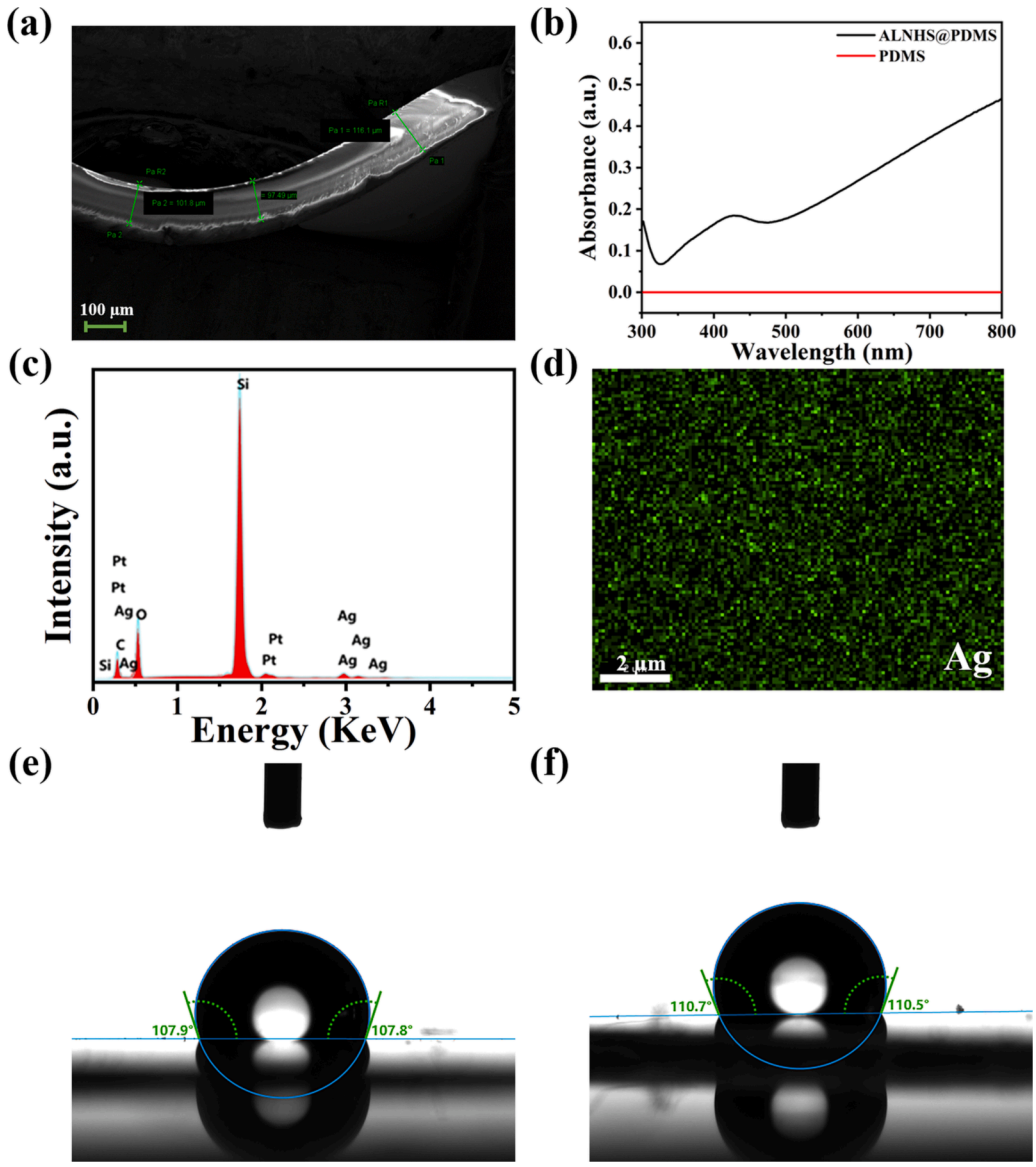


Fig. 3. (a) The cross-sectional view SEM image and (b) UV–vis spectrum of ALNHS-45@PDMS film. (c) The EDS spectra and (d) EDS mapping of the ALNHS-45@PDMS film. Contact angles of a water droplet on the surface of (e) the pure PDMS film and (f) the ALNHS-45@PDMS film.

adsorbed on the flexible ALNHS-45@PDMS film. It can be seen that the SERS intensity gradually decreases with a decrease in R6G concentration. The characteristic Raman peaks of R6G at concentration as low as 10^{-7} M can be still identified and distinguished, indicating that the ALNHS-45@PDMS film has high SERS activity. In addition, the calibration curve of Raman intensity at 1510 cm^{-1} versus logarithmic concentration in the range of 10^{-3}-10^{-7} M shows a good linear relationship ($R^2 = 0.992$), as shown in Fig. 4c, indicating that the ALNHS-45@PDMS film enables quantitative analysis capability. To further evaluate the SERS performance of the ALNHS-45@PDMS film, its enhancement factor (EF) was calculated according to the following formula: $EF=(I_{SERS}/C_{SERS})/(I_{NR}/C_{NR})$ [50]. Here, I_{SERS} and I_{NR} are peak intensities in the SERS spectrum and the normal Raman spectrum, respectively; C_{SERS} and C_{NR} are the respective probe concentrations in the SERS and the normal Raman measurement. As shown in Fig. 4d, when the R6G solution (10^{-1} M) was dropped onto the pure PDMS film, the peak intensity at 1510 cm^{-1} is very low (800 a.u.). In contrast to the pure PDMS film, the SERS intensity of R6G solution (10^{-7} M) on the ALNHS-45@PDMS film is significantly enhanced and reaches 4191 a.u. The EF for the intense peaks of R6G at 1510 cm^{-1} was thus calculated to be 5.2×10^6, revealing an excellent SERS enhancement of the ALNHS-45@PDMS film. The high sensitivity of the ALNHS-45@PDMS film can be mainly attributed to the existence of high-density hot spots resulting from multiple plasmon couplings on the substrate. The hot spots can be generated in between the adjacent Ag NPs on a single microlabyrinth (Type A) and in close microlabyrinths due to interparticle plasmon coupling (Type B).

3.3. Uniformity and reproducibility of the ALNHS-45@PDMS film

Uniformity and reproducibility are two important factors for reliable quantitative SERS analysis in actual applications. To investigate the uniformity of the ALNHS-45@PDMS film, 5 μL of 10^{-5} M R6G solution was dropped onto 10 different locations at the center, middle and edge of the ALNHS-45@PDMS film. In each location, ten SERS measurements were carried out. Fig. 5a shows the SERS spectra of R6G collected at 100 randomly selected spots on the ALNHS-45@PDMS film. One can see that the line shapes and intensities of the Raman bands were fairly consistent. The relative standard deviation (RSD) value of the intensity at 1510 cm^{-1} was calculated to 7.99%, as demonstrated in

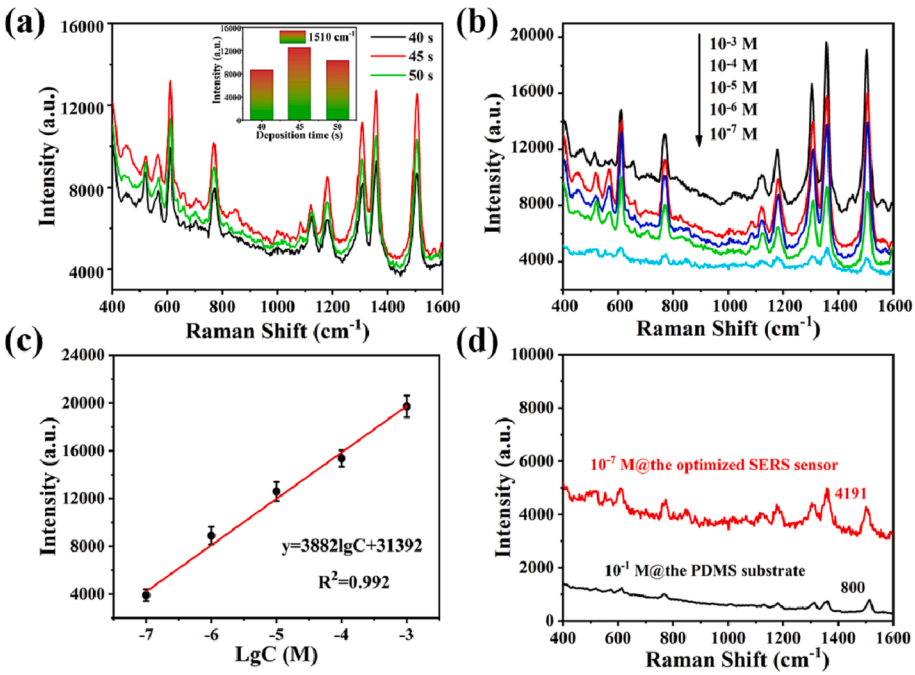


Fig. 4. (a) SERS spectra of 10^{-5} M R6G collected on the ALNHS@PDMS films with different sputtering times. The inset shows the SERS intensity at 1510 cm^{-1} as a function of sputtering time. (b) SERS spectra of R6G molecules from 10^{-3} to 10^{-7} M on the ALNHS-45@PDMS film. (c) Plot of Raman intensity at 1510 cm^{-1} versus the logarithm of R6G concentrations. (d) SERS spectra of 10^{-7} M R6G on the ALNHS-45@PDMS film and Raman spectrum of 10^{-1} M R6G on the pure PDMS film.

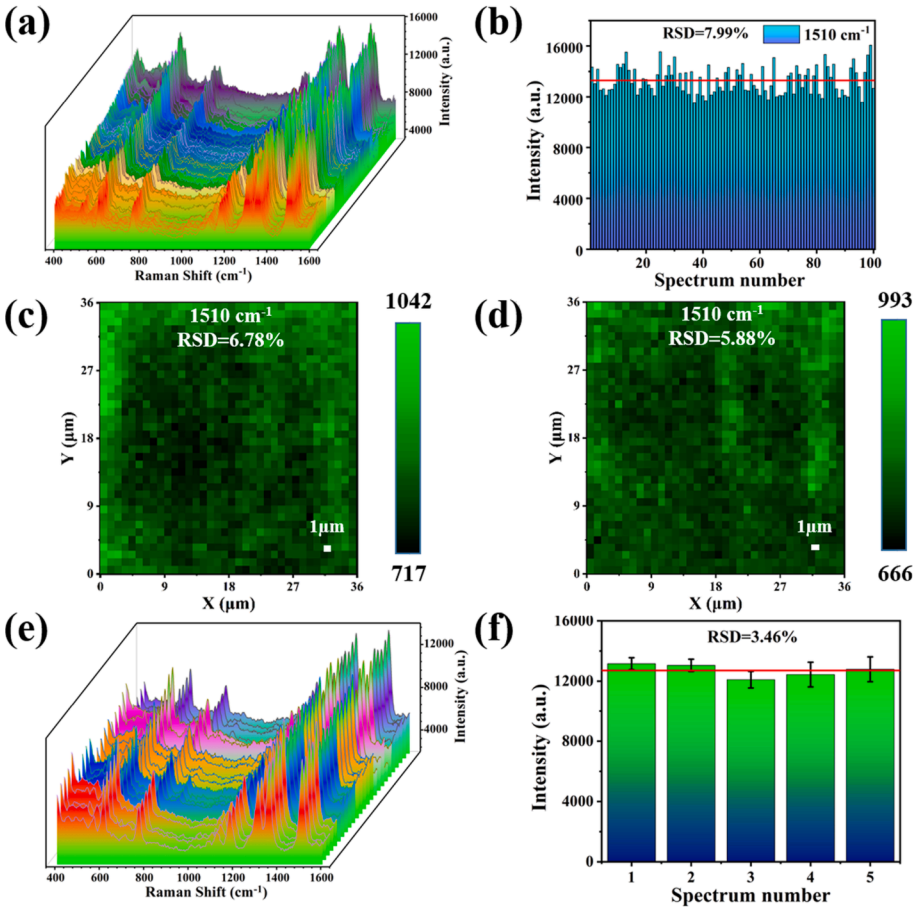


Fig. 5. (a) SERS spectra of 10^{-5} M R6G from 100 random spots on the ALNHS-45@PDMS film. (b) The corresponding SERS intensity at 1510 cm^{-1} with RSD value of 7.99%. (c-d) Raman mappings of 10^{-7} M R6G at 1510 cm^{-1} with RSD value of 6.78%, and 5.88% obtained from two positions on the same ALNHS-45@PDMS substrate. (e) SERS spectra of 10^{-5} M R6G from 5 batches of ALNHS-45@PDMS substrate. (f) The corresponding SERS intensity at 1510 cm^{-1} with RSD value of 3.46%.

Fig. 5b, indicating that the ALNHS-45@PDMS film possesses good uniformity. The SERS mapping measurements of two 36 μm × 36 μm regions were also implemented to evaluate the signal homogeneity of the ALNHS-45@PDMS film, as depicted in Fig. 5c, d. The corresponding RSD values of the peak intensity at 1510 cm^{-1} were 6.78% and 5.88%, which further demonstrates the remarkable uniformity of the ALNHS-45@PDMS film. In order to assess batch-to-batch reproducibility, we collected SERS spectra of R6G from five different batches under the same measurement condition. For each substrate, five random sites were measured, and the SERS spectra of R6G are shown in Fig. 5e. It is obvious that the SERS signals were highly reproducible from batch to batch by comparing the intensity and shape of the Raman peaks. The RSD value for the peak at 1510 cm^{-1} is 3.46%, as shown in Fig. 5f, indicating excellent batch-to-batch reproducibility of the ALNHS-45@PDMS films. These results clearly confirm that the ALNHS-45@PDMS films have high uniformity and excellent reproducibility, which may be attributed to high-density hot spots induced by ALNHS and the fabrication process repeatability.

3.4. Mechanical stability of the flexible ALNHS-45@PDMS film

To achieve non-destructive detection of contaminants on nonplanar surfaces in practical applications, the mechanical durability of flexible SERS substrates is profoundly important. Hence, it is necessary to study the influence of mechanical stimuli on the SERS activity of flexible SERS substrates. Here, the mechanical property of the flexible ALNHS-45@PDMS film was assessed by conducting bending and twisting test, in which the substrates were bent in half and twisted to ~180° for 100 cycles. The SERS spectra of R6G (10^{-5} M) was recorded for every 10 mechanical deformations, as shown in the insets of Fig. 6a, c. After bending and torsion of 100 cycles, the SERS intensity of R6G at peak 1510 cm^{-1} shows no significant change, as demonstrated in Fig. 6b, d. The mechanical stability of flexible ALNHS-45@PDMS film could be attributed to the good flexibility of the substrate as shown in Fig. 1b-d and well adhesion between the ALNHS and the PDMS film. The SEM images of flexible ALNHS-45@PDMS films confirm that the plasmonic structures were well maintained after 100 cycles of bending and twisting, as demonstrated in the insets of Fig. 6b, d. These results demonstrate that the flexible ALNHS-45@PDMS film has the robust adhesion between the plasmonic ALNHS and the thin PDMS film. Additionally, the scotch-tape peel test was also carried out to investigate the adhesion between them. Fig. 6e shows the SERS spectra of 10^{-5} M R6G on the flexible ALNHS-45@PDMS film after peel tests. After repeated three peel tests, the flexible ALNHS-45@PDMS film still maintains the stable SERS intensity of R6G at 1510 cm^{-1}. The SEM image of the surface morphology of the flexible ALNHS-45@PDMS film (inset of Fig. 6f) indicates that there was no loss of plasmonic structures after the scotch tape tests, evidencing the good adhesion between the ALNHS and the PDMS films. These results indicate that the flexible ALNHS-45@PDMS film has good mechanical durability, meeting the demanding performance needs of the flexible SERS substrate for in situ detection of pollutants on curved substrates.

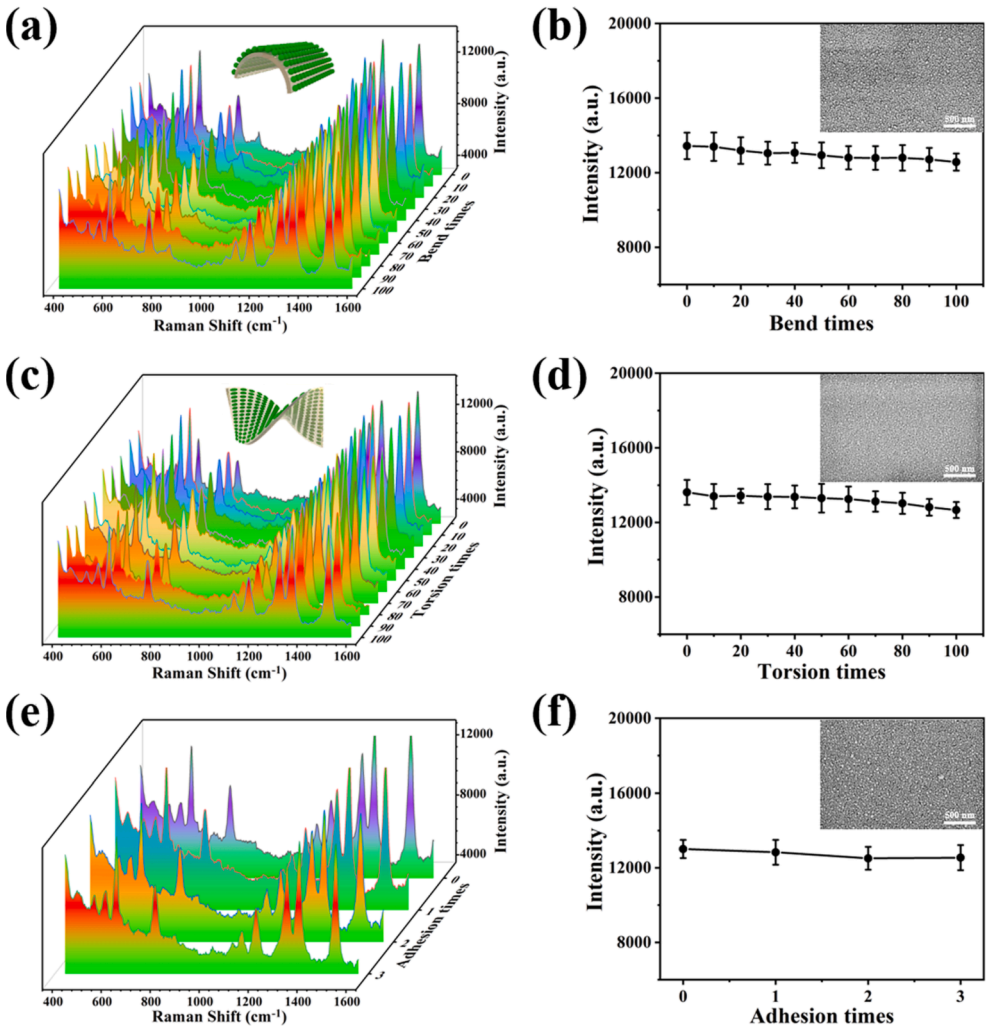


Fig. 6. (a) SERS spectra of 10^{-5} M R6G and (b) corresponding signal intensity at 1510 cm^{-1} after bending the flexible ALNHS-45@PDMS substrate in 100 cycles. (c) SERS spectra of 10^{-5} M R6G and (d) corresponding signal intensity at 1510 cm^{-1} after twisting the flexible ALNHS-45@PDMS substrate in 100 cycles. (e) SERS spectra of 10^{-5} M R6G and (f) corresponding signal intensity at 1510 cm^{-1} during adhesion test. The insets in (b), (d), and (f) show SEM images of ALNHS-45@PDMS film after bending, twisting, and scotch-tape peel tests.

3.5. Storage stability of the ALNHS-45@PDMS film

The stability of SERS substrates against storing time also needs to be considered for practical application in routine analysis. The storage stability of the flexible ALNHS-45@PDMS film over time was tested under open air and protected condition. As illustrated in Fig. 7a, the SERS intensity of R6G at 1510 cm^{-1} recorded from the ALNHS-45@PDMS film stored in air condition reduced by 6.8% after 21 days. In contrast, the SERS intensity of R6G at 1510 cm^{-1} on the ALNHS-45@PDMS film protected with a cling film attenuated by 5.4% after 21 days (Fig. 7b). The above results demonstrate that the flexible ALNHS-45@PDMS film demonstrates good reliability, and the cling film as a protective barrier can improve storage stability to a certain extent.

3.6. Comparison of SERS activity under different irradiation modes

To achieve in situ detection, exciting and collecting the SERS signal from the back side of the transparent and flexible substrate should be guaranteed. To this end, the estimation of the bidirection-activatable property for the ALNHS-45@PDMS film was investigated through two different measurement modes, e.g. front-side mode and back-side mode, as shown in Fig. 8a, b. Two different measurement modes of MG and CV solutions with various concentrations were conducted on the as-prepared transparent and flexible SERS substrates, and the obtained SERS spectra are depicted in Fig. 8c, d. The typical peaks of MG and CV are consistent with previous papers [51–53]. It can be seen that the peak intensities of MG and CV obtained from both sides of the ALNHS-45@PDMS film were almost the same, demonstrating that the as-prepared ALNHS-45@PDMS films possess in situ detection capability.

3.7. In situ detection of MG on apple and tomato skin

Due to the excellent flexibility, good transparency and bi-directional activation property, it is expected that the ALNHS-45@PDMS film could serve as a high-quality flexible and transparent SERS substrate for rapid, in situ detection of contaminants on curved surfaces. To validate this concept, the MG solutions with different concentrations were dropped onto the apple and tomato peels, and then completely dried at room temperature to simulate the actual scene. After that, we covered a small piece of the as-prepared flexible SERS substrate on them with ALNHS facing the contaminated skin, and then collected SERS signals from the backside of the ALNHS-45@PDMS films via a portable Raman spectrometer, as shown in Fig. 9a, d. Since the total thickness of the ALNHS-45@PDMS film is thin, the flexible SERS substrate can provide conformal contacts with the surface of objects with no further supports, which enables the close proximity between hot spots and analytes, and therefore gives rise to a high SERS enhancement. Fig. 9b, e present the SERS spectra of MG solutions with concentrations in the range of 10^{-2} to 10^{-6} M on the apple and tomato surfaces, respectively. The characteristic band of the MG solution with the concentration as low as 10^{-6} M can still be clearly identified, demonstrating that the ALNHS-45@PDMS film can act as a flexible and transparent SERS substrate with highly sensitive sensing capability for in situ detection. This significant amplification of Raman signals may be attributed to the close contact between the ALNHS with abundantly available SERS hot spots and MG molecules on the contaminated surface. The corresponding peak intensity of MG at 1616 cm^{-1} versus the logarithmic concentration of MG displays an excellent linear correlation with respective $R^2 = 0.993$ and $R^2 = 0.992$, as shown in Fig. 9c, f. The good linear correlation guarantees the suitability of ALNHS-45@PDMS film in quantitative determination for in situ contamination detection. The above results demonstrate that the as-prepared ALNHS-45@PDMS film, integrated with a portable Raman spectrometer, provides a good sensing ability for in situ detection and can be readily adopted for real-world applications.

4. Conclusion

In summary, a large-area, free-standing, flexible and transparent SERS substrate was prepared by using the floating-on-water method and magnetron sputtering technology. The as-prepared flexible and transparent SERS substrate consists of Ag microlabyrinth/nanoparticles hierarchical structures and large-area thin PDMS film. The optimized ALNHS@PDMS SERS substrate with plentiful multiple-type hot spots provided high sensitivity, good uniformity, superior batch-to-batch reproducibility, excellent mechanical stability and long-term stability. The enhancement effect of the ALNHS@PDMS film in both front-side and back-side measurement modes was also demonstrated. The rapid in situ detection ability of this SERS substrate was validated via the direct detection of MG at the level of 10^{-6} M on apple and tomato skin by a portable Raman spectrometer. In view of its high sensitivity, superior reproducibility, excellent mechanical stability, in situ detection capability as well as the facile route for large-scale preparation, the ALNHS@PDMS film integrated with a portable Raman spectrometer holds great potentials in POCT applications for rapid, real-time, and on-site detection.

CRediT authorship contribution statement

Meng Sun: Methodology, Writing – original draft. **Houjia Zhang:** Methodology. **Hefu Li:** Supervision, Project administration, Funding acquisition. **Xuehui Hao:** Methodology, Funding acquisition. **Changzheng Wang:** Methodology, Supervision. **Lijun Li:** Formal analysis. **Zhenshan Yang:** Writing – review & editing. **Cunwei Tian:** Methodology, Supervision.

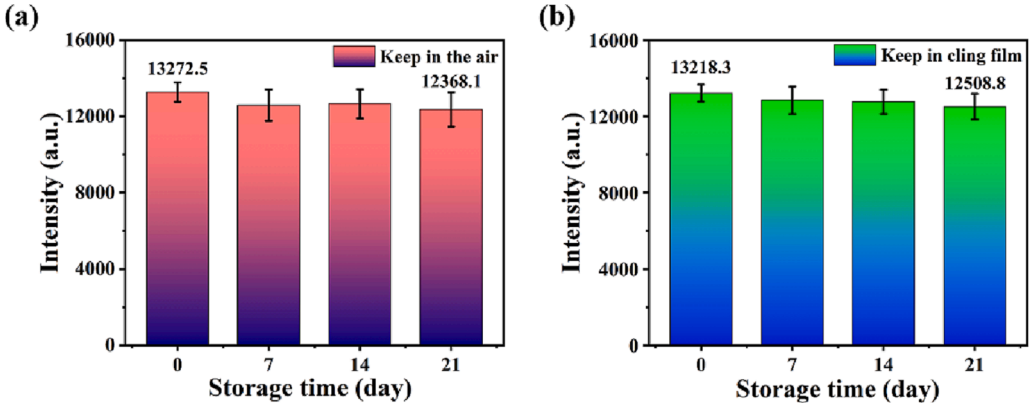


Fig. 7. SERS intensity of R6G (10^{-5} M) at 1510 cm^{-1} on the ALNHS-45@PDMS substrate (a) without and (b) with a cling film protection at different times.

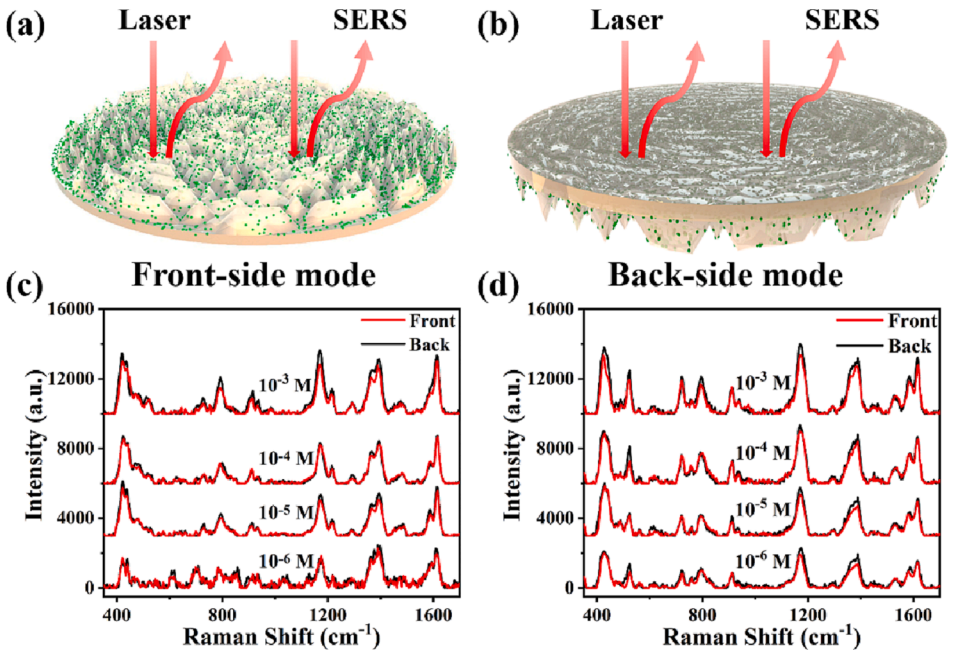


Fig. 8. Schematic illustration of SERS measurements under (a) front-side and (b) back- side excitation mode. Comparison of SERS spectra of (c) MG and (d) CV with concentrations ranging from 10^{-3} to 10^{-6} M obtained from both sides of the ALNHS-45@PDMS film.

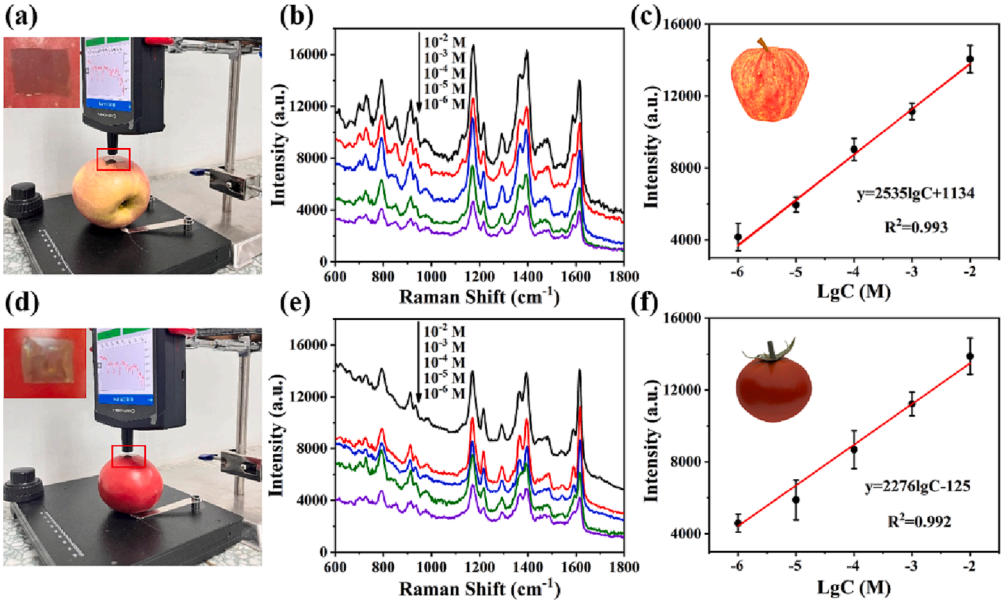


Fig. 9. The real-time and in situ detection of MG on (a) apple and (d) tomato surface. The insets respectively showing the ALNHS-45@PDMS film tightly wrapped apple and tomato skin. SERS spectra of MG with concentration ranging from 10^{-2} to 10^{-6} M on the surface of (b) apple and (e) tomato. The fitting curve plotted between the average intensity of SERS signal at 1616 cm^{-1} against the logarithmic concentration of MG on (c) apple and (f) tomato surface.

Declaration of Competing Interest

The authors declare that they have no known competing financial interests or personal relationships that could have appeared to influence the work reported in this paper.

Data availability

Data will be made available on request.

Acknowledgments

The authors gratefully acknowledge funding supports from the Natural Science Foundation of Shandong Province (Grant No. ZR2021MF097, ZR2020QE026); China Postdoctoral Science Foundation (Grant No. 2018 M642289); Liaocheng University Start-up Fund for Doctoral Scientific Research (Grant No. 318051542).

References

[1] D.R. Zhang, H.B. Pu, L.J. Huang, D.-W. Sun, Advances in flexible surface-enhanced Raman scattering (SERS) substrates for nondestructive food detection:

Fundamentals and recent applications, Trends Food Sci. Tech. 109 (2021) 690–701, https://doi.org/10.1016/j.tifs.2021.01.058.
[2] X.F. Liu, J.M. Ma, P.F. Jiang, J.L. Shen, R.W. Wang, Y. Wang, G.L. Tu, Large-Scale flexible surface-enhanced Raman scattering (SERS) sensors with high stability and signal homogeneity, ACS Appl. Mater. Interfaces 12 (2020) 45332–45341, https://doi.org/10.1021/acsami.0c13691.
[3] H.M. Sun, X.T. Li, Z.Y. Hu, C.J. Gu, D. Chen, J. Wang, B. Li, T. Jiang, X.F. Zhou, Hydrophilic-hydrophobic silver nanowire-paper based SERS substrate for in-situ detection of furazolidone under various environments, Appl. Surf. Sci. 556 (2021) 149748, https://doi.org/10.1016/j.apsusc.2021.149748.
[4] X. He, X. Zhou, Y. Liu, X.L. Wang, Ultrasensitive, recyclable and portable microfluidic surface-enhanced Raman scattering (SERS) biosensor for uranyl ions detection, Sensor. Actuat. B Chem. 311 (2020) 127676, https://doi.org/10.1016/j.snb.2020.127676.
[5] X. Pan, L.H. Li, H.D. Lin, J.Y. Tan, H.T. Wang, M.L. Liao, C.J. Chen, B.B. Shan, Y. F. Chen, M. Li, A graphene oxide-gold nanostar hybrid based-paper biosensor for label-free SERS detection of serum bilirubin for diagnosis of jaundice, Biosens. Bioelectron. 145 (2019) 111713, https://doi.org/10.1016/j.bios.2019.111713.
[6] Y.L. Wang, C. Zhao, J.J. Wang, X. Luo, L.J. Xie, S.J. Zhan, J.M. Kim, X.Z. Wang, X. J. Liu, Y.B. Ying, Wearable plasmonic-metasurface sensor for noninvasive and universal molecular fingerprint detection on biointerfaces, Sci. Adv. 7 (2021) 4553, https://doi.org/10.1126/sciadv.abe45.
[7] Y. Shi, W.S. Wang, J.H. Zhan, A positively charged silver nanowire membrane for rapid on-site swabbing extraction and detection of trace inorganic explosives using a portable Raman spectrometer, Nano Res. 9 (2016) 2487–2497, https://doi.org/10.1007/s12274-016-1135-5.
[8] Z.B. Li, G.W. Meng, Q. Huang, X.Y. Hu, X. He, H.B. Tang, Z.W. Wang, F.D. Li, Ag nanoparticle-grafted PAN-nanohump array films with 3D high-density hot spots as flexible and reliable SERS substrates, Small 11 (2015) 5452–5459, https://doi.org/10.1002/smll.201501505.
[9] M. Pradhan, J. Chowdhury, S. Sarkar, A.K. Sinha, T. Pal, Hierarchical gold flower with sharp tips from controlled galvanic replacement reaction for high surface enhanced Raman scattering activity, J. Phys. Chem. C 116 (2012) 24301–24313, https://doi.org/10.1021/jp306330p.
[10] H.M. Jin, J.Y. Kim, M. Heo, S.J. Jeong, B.H. Kim, S.K. Cha, K.H. Han, J.H. Kim, G. G. Yang, J. Shin, S.O. Kim, Ultralarge area sub-10 nm plasmonic nanogap array by block copolymer self-assembly for reliable high-sensitivity SERS, ACS Appl. Mater. Interfaces 10 (2018) 44660–44667, https://doi.org/10.1021/acsami.8b17325.
[11] X. Wan, S.-C. Huang, S. Hu, S. Yan, B. Ren, Fundamental understanding and applications of plasmon-enhanced Raman spectroscopy, Nat. Rev. Phys. 2 (2020) 253–271, https://doi.org/10.1038/s42254-020-0171-y.
[12] Y.-J. Oh, M. Kang, M. Park, K.-H. Jeong, Engineering hot spots on plasmonic nanopillar arrays for SERS: A Review, BioChip J. 10 (2016) 297–309, https://doi.org/10.1007/s13206-016-0406-2.
[13] H.-Y. Wu, C.J. Choi, B.T. Cunningham, Plasmonic nanogap-enhanced Raman scattering using a resonant nanodome array, Small 8 (2012) 2878–2885, https://doi.org/10.1002/smll.201200712.
[14] J. Bär, A. de Barros, D.H.S. de Camargo, M.P. Pereira, L. Merces, F.M. Shimizu, F. A. Sigoli, C.C.B. Bufon, I.O. Mazali, Silicon microchannel-driven Raman scattering enhancement to improve gold nanorod functions as a SERS substrate toward single-molecule detection, ACS Appl. Mater. Interfaces 13 (2021) 36482–36491, https://doi.org/10.1021/acsami.1c08480.
[15] Q. Fu, Z.B. Zhan, J.X. Dou, X.Z. Zheng, R. Xu, M.H. Wu, Y. Lei, Highly reproducible and sensitive SERS substrates with Ag inter-nanoparticle gaps of 5 nm fabricated by ultrathin aluminum mask technique, ACS Appl. Mater. Interfaces 7 (2015) 13322–13328, https://doi.org/10.1021/acsami.5b01524.
[16] C. Zhang, C. Ji, J. Yu, Z. Li, Z.X. Li, C.H. Li, S.C. Xu, W.F. Li, B.Y. Man, X.F. Zhao, MoS_2-based multiple surface plasmonic coupling for enhanced surface-enhanced Raman scattering and photoelectrocatalytic performance utilizing the size effect, Opt. Express 29 (2021) 38768–38780, https://doi.org/10.1364/OE.441176.
[17] M. Zarei, Advances in point-of-care technologies for molecular diagnostics, Biosens. Bioelectron. 98 (2017) 494–506, https://doi.org/10.1016/j.bios.2017.07.024.
[18] K.C. Xu, R. Zhou, K.H. Takei, M.H. Hong, Toward flexible surface-enhanced Raman scattering (SERS) sensors for point-of-care diagnostics, Adv. Sci. 6 (2019) 1900925, https://doi.org/10.1002/advs.201900925.
[19] M.S.S. Bharati, V.R. Soma, Flexible SERS substrates for hazardous materials detection: Recent advances, Opto-Electron. Adv. 4 (2021) 210048, https://doi.org/10.29026/oea.2021.210048.
[20] H.Y. Liu, P.N. Zhao, W.L. Xiu, L.N. Zhang, P.H. Zhu, S.G. Ge, J.H. Yu, SERS paper slip based on 3D dendritic gold nanomaterials coupling with urchin-like nanoparticles for rapid detection of thiram, Sensor. Actuat. B Chem. 355 (2022) 131264, https://doi.org/10.1016/j.snb.2021.131264.
[21] F.Y. Zeng, W.D. Duan, B. Zhu, T.T. Mu, L.Q. Zhu, J.H. Guo, X. Ma, Paper-based versatile surface-enhanced Raman spectroscopy chip with smartphone-based Raman analyzer for point-of-care application, Anal. Chem. 91 (2019) 1064–1070, https://doi.org/10.1021/acs.analchem.8b04441.
[22] L.Y. Chen, B.B. Ying, P.F. Song, X.Y. Liu, A nanocellulose-paper-based SERS multiwell plate with high sensitivity and high signal homogeneity, Adv. Mater. Interfaces 6 (2019) 1901346, https://doi.org/10.1002/admi.201901346.
[23] K.Q. Wang, D.-W. Sun, H.B. Pu, Q.Y. Wei, Polymer multilayers enabled stable and flexible Au@Ag nanoparticle array for nondestructive SERS detection of pesticide residues, Talanta 223 (2021) 121782, https://doi.org/10.1016/j.talanta.2020.121782.
[24] N.R. Barveen, T.-J. Wang, Y.-H. Chang, Photochemical synthesis of Au nanostars on PMMA films by ethanol action as flexible SERS substrates for in-situ detection of antibiotics on curved surfaces, Chem. Eng. J. 431 (2022) 134240, https://doi.org/10.1016/j.cej.2021.134240.
[25] Y.M. Chen, F.Y. Ge, S.Y. Guang, Z.S. Cai, Low-cost and large-scale flexible SERS-cotton fabric as a wipe substrate for surface trace analysis, Appl. Surf. Sci. 436 (2018) 111–116, https://doi.org/10.1016/j.apsusc.2017.11.288.
[26] W. Gao, J.T. Xu, C. Cheng, S. Qiu, S.X. Jiang, Rapid and highly sensitive SERS detection of fungicide based on flexible "wash free" metallic textile, Appl. Surf. Sci. 512 (2020) 144693, https://doi.org/10.1016/j.apsusc.2019.144693.
[27] Y.D. Wang, M.Y. Zhang, L. Feng, B. Dong, T. Xu, D. Li, L. Jiang, L.F. Chi, Tape-imprinted hierarchical lotus seedpod-like arrays for extraordinary surface-enhanced Raman spectroscopy, Small 15 (2019) 1804527, https://doi.org/10.1002/smll.201804527.
[28] J.M. Chen, Y.J. Huang, P. Kannan, L. Zhang, Z.Y. Lin, J.W. Zhang, T. Chen, L. H. Guo, Flexible and adhesive surface enhance Raman scattering active tape for rapid detection of pesticide residues in fruits and vegetables, Anal. Chem. 88 (2016) 2149–2155, https://doi.org/10.1021/acs.analchem.5b03735.
[29] H.Q. Liu, Y.N. He, K.Z. Cao, Flexible surface-enhanced Raman scattering substrates: A review on constructions, applications, and challenges, Adv. Mater. Interfaces 8 (2021) 2100982, https://doi.org/10.1002/admi.202100982.
[30] L.P. Xie, H. Zeng, J.X. Zhu, Z.L. Zhang, H.-B. Sun, W. Xia, Y.N. Du, State of the art in flexible SERS sensors toward label-free and onsite detection: From design to applications, Nano Res. 15 (2022) 4374–4394, https://doi.org/10.1007/s12274-021-4017-4.
[31] K.Q. Wang, D.-W. Sun, H.B. Pu, Q.Y. Wei, L.J. Huang, Stable, flexible, and high-performance SERS chip enabled by a ternary film-packaged plasmonic nanoparticle Array, ACS Appl. Mater. Interfaces 11 (2019) 29177–29186, https://doi.org/10.1021/acsami.9b09746.
[32] N.C. Creedon, P. Lovera, A. Furey, A. O'Riordan, Transparent polymer-based SERS substrates templated by a soda can, Sensor. Actuat. B Chem. 259 (2018) 64–74, https://doi.org/10.1016/j.snb.2017.12.039.
[33] Y. Ma, Y.Y. Du, Y. Chen, C.J. Gu, T. Jiang, G.D. Wei, J. Zhou, Intrinsic Raman signal of polymer matrix induced quantitative multiphase SERS analysis based on stretched PDMS film with anchored Ag nanoparticles/Au nanowires, Chem. Eng. J. 381 (2020) 122710, https://doi.org/10.1016/j.cej.2019.122710.
[34] Y.C. Wang, Y.H. Jin, X.Y. Xiao, T.F. Zhang, H.T. Yang, Y.D. Zhao, J.P. Wang, K. L. Jiang, S.S. Fan, Q.Q. Li, Flexible, transparent and highly sensitive SERS substrates with cross-nanoporous structures for fast on-site detection, Nanoscale 10 (2018) 15195–15204, https://doi.org/10.1039/c8nr01628c.
[35] P. Wu, L.-B. Zhong, Q. Liu, X. Zhou, Y.-M. Zheng, Polymer induced one-step interfacial self-assembly method for the fabrication of flexible, robust and free-standing SERS substrates for rapid on-site detection of pesticide residues, Nanoscale 11 (2019) 12829–12836, https://doi.org/10.1039/c9nr02851j.
[36] Z.Y. Li, X. Huang, G. Lu, Recent developments of flexible and transparent SERS substrates, J. Mater. Chem. C 8 (2020) 3956–3969, https://doi.org/10.1039/d0tc00002g.
[37] L.M. Li, W.S. Chin, Rapid fabrication of a flexible and transparent Ag nanocubes@PDMS film as a SERS substrate with high performance, ACS Appl. Mater. Interfaces 12 (2020) 37538–37548, https://doi.org/10.1021/acsami.0c07178.
[38] B. Fortun, T. Inose, S. Uezono, S. Toyouchi, K. Umemoto, S. Sekine, Y. Fujita, M. Ricci, G. Lu, A. Masuhara, J.A. Hutchison, L. Latterini, H. Uji-i, In situ synthesis of Au-shelled Ag nanoparticles on PDMS for flexible, long-life, and broad spectrum-sensitive SERS substrates, Chem. Commun. 53 (2017) 11298–11301, https://doi.org/10.1039/c7cc05420c.
[39] B. Fortuni, Y. Fujita, M. Ricci, T. Inose, R. Aubert, G. Lu, J.A. Hutchison, J. Hofkens, L. Latterini, H. Uji-I, A novel method for in situ synthesis of SERS-active gold nanostars on polydimethylsiloxane film, Chem. Commun. 53 (2017) 5121–5124, https://doi.org/10.1039/c7cc01776f.
[40] A. Alyami, A.J. Quinn, D. Iacopino, Flexible and transparent surface enhanced Raman scattering (SERS)-active Ag NPs/PDMS composites for in-situ detection of food contaminants, Talanta 201 (2019) 58–64, https://doi.org/10.1016/j.talanta.2019.03.115.
[41] S. Park, J. Lee, H. Ko, Transparent and flexible surface-enhanced Raman scattering (SERS) sensors based on gold nanostar arrays embedded in silicon rubber film, ACS Appl. Mater. Interfaces 9 (2017) 44088–44095, https://doi.org/10.1021/acsami.7b14022.
[42] P. Wang, L. Wu, Z.C. Lu, Q. Li, W.M. Yin, F. Ding, H.Y. Han, Gecko-inspired nanotentacle surface-enhanced Raman spectroscopy substrate for sampling and reliable detection of pesticide residues in fruits and vegetables, Anal. Chem. 89 (2017) 2424–2431, https://doi.org/10.1021/acs.analchem.6b04324.
[43] Y. Ma, H.M. Liu, Y. Chen, C.J. Gu, G.D. Wei, T. Jiang, Improved lateral flow strip based on hydrophilic-hydrophobic SERS substrate for ultra-sensitive and quantitative immunoassay, Appl. Surf. Sci. 529 (2020) 147121, https://doi.org/10.1016/j.apsusc.2020.147121.
[44] C.P. Zhang, S. Chen, J.L. Wang, Z.Y. Shi, L.A. Du, Reproducible flexible SERS substrates inspired by bionic micro-nano hierarchical structures of rose petals, Adv. Mater. Interfaces 9 (2022) 2102468, https://doi.org/10.1002/admi.202102468.
[45] J. Cai, Z.H. Wang, M.J. Wang, D.Y. Zhang, Au nanoparticle-grafted hierarchical pillars array replicated from diatom as reliable SERS substrates, Appl. Surf. Sci. 541 (2021) 148374, https://doi.org/10.1016/j.apsusc.2020.148374.
[46] D. Kim, S.-H. Kim, J.Y. Park, Floating-on-water fabrication method for thin polydimethylsiloxane membranes, Polymers 11 (2019) 1264, https://doi.org/10.3390/polym11081264.
[47] S.J. Li, K. Wu, H.Z. Yuan, J.Y. Zhang, G. Liu, J. Sun, Formation of wrinkled patterns in metal films deposited on elastic substrates: Tunability and wettability, Surf. Coat. Tech. 362 (2019) 35–43, https://doi.org/10.1016/j.surfcoat.2019.01.088.

[48] C.D. Liu, J. Li, F.C. Lei, Y.S. Wei, Z. Li, C. Zhang, Q.Q. Peng, J. Yu, B.Y. Man, SERS substrate with wettability difference for molecular self-concentrating detection, Nanotechnology 32 (2021) 375603, https://doi.org/10.1088/1361-6528/ac0665/meta.

[49] H.B. Sun, H. Liu, Y.Y. Wu, A green, reusable SERS film with high sensitivity for in-situ detection of thiram in apple juice, Appl. Surf. Sci. 416 (2017) 704–709, https://doi.org/10.1016/j.apsusc.2017.04.159.

[50] T.-J. Wang, N.R. Barveen, Z.-Y. Liu, C.-H. Chen, M.-H. Chou, Transparent, flexible plasmonic Ag NP/PMMA substrates using chemically patterned ferroelectric crystals for detecting pesticides on curved surfaces, ACS Appl. Mater. Interfaces 13 (2021) 34910–34922, https://doi.org/10.1021/acsami.1c08233.

[51] L. Wu, L.C. Cui, J. Guo, Y. Peng, J.H. Zou, B.J. Yu, L.M. Qian, Rapid and flexible construction of inverted silicon architectures with nanogaps as high-performance SERS substrates, Appl. Surf. Sci. 594 (2022) 153429, https://doi.org/10.1016/j.apsusc.2022.153429.

[52] H.-Y. Chen, M.-H. Lin, C.-Y. Wang, Y.-M. Chang, S. Gwo, Large-scale hot spot engineering for quantitative SERS at the single-molecule scale, J. Am. Chem. Soc. 137 (2015) 13698–13705, https://doi.org/10.1021/jacs.5b09111.

[53] C. Zhang, Z.X. Li, S. Qiu, W.X. Lu, M.R. Shao, C. Ji, G.C. Wang, X.F. Zhao, J. Yu, Z. Li, Highly ordered arrays of hat-shaped hierarchical nanostructures with different curvatures for sensitive SERS and plasmon-driven catalysis, Nanophotonics 11 (2022) 33–44, https://doi.org/10.1515/nanoph-2021-0476.